Protein Motifs Involved in Coenzyme Interaction and Enzymatic Efficiency in *Anabaena* Ferredoxin-NADP$^+$ Reductase[†,‡]

José R. Peregrina,[§,||] Beatriz Herguedas,[§,||] Juan A. Hermoso,[⊥] Marta Martínez-Júlvez,*[,§] and Milagros Medina*[,§]

Departamento de Bioquímica y Biología Molecular y Celular, Facultad de Ciencias, and Institute of Biocomputation and Physics of Complex Systems, Universidad de Zaragoza, 50009 Zaragoza, Spain, and Grupo de Cristalografía Molecular y Biología Estructural, Instituto Química-Física Rocasolano, Consejo Superior de Investigaciones Científicas, Serrano 119, 28006 Madrid, Spain

Received November 11, 2008; Revised Manuscript Received February 13, 2009

ABSTRACT: Ferredoxin-NADP$^+$ reductases (FNRs) must determine the coenzyme specificity and allow the transient encounter between N5 of its flavin cofactor and C4 of the coenzyme nicotinamide for efficient hydride transfer. Combined site-directed replacements in different putative determinants of the FNR coenzyme specificity were simultaneously produced. The resulting variants were structurally and functionally analyzed for their binding and hydride transfer abilities to the FNR physiological coenzyme NADP$^+$/H, as well as to NAD$^+$/H. The previously studied Y303S mutation is the only one that significantly enhances specificity for NAD$^+$. Combination of mutations from the pyrophosphate or 2′-phosphate regions, even including Y303S, does not improve activity with NAD$^+$, despite structures of these FNRs show how particular coenzyme-binding regions resembled motifs found in NAD$^+$/H-dependent enzymes of the FNR family. Therefore, the "rational approach" did not succeed well, and coenzyme specificity redesign in the FNR family will be more complex than that anticipated in other NADP$^+$/NAD$^+$ families.

The only structural difference between NADP$^+$/H and NAD$^+$/H is the presence of a 2′-phosphate (2′-P) in the NADP$^+$/H molecule, but usually pyridine nucleotide-dependent enzymes distinguish between these coenzymes (*1*−*5*). Despite the fact that specificity determinants have been established for different NAD(P)$^+$/H-dependent flavoenzymes and attempts to redesign specificity have been reported (*3, 6*−*10*), the mechanism of coenzyme recognition is not completely understood (*11*). The plastidic ferredoxin-NADP$^+$ reductase (FNR,[1] EC 1.18.1.2) catalyzes the efficient electron/hydride transfer between low-potential one-electron carriers and NADP$^+$/H, while bacterial FNRs generally exhibit slower turnovers (*12*). Plastidic FNRs catalyze the transfer of two electrons from two independent reduced ferredoxins (Fd) [or flavodoxins (Fld)] to NADP$^+$ (*13*). This process is reversible, and FNR is highly specific for NADP$^+$/H versus NAD$^+$/H (*2, 14*). Additionally, the folding of FNR is the prototype of a family containing both NAD$^+$/H- and NADP$^+$/H-dependent members (*15*−*18*).

Several residues have been reported to determine coenzyme binding, specificity, and enzymatic efficiency in FNR (*2, 5, 11, 14, 19, 20*). Three main regions allocate them: the binding sites of the 2′-P-AMP and the pyrophosphate bridge of NADP$^+$/H and the position occupied by the C-terminal residue where the nicotinamide portion of NADP$^+$ (NMN) must bind for hydride transfer (HT) (Figure 1A) (*2, 5, 11, 19, 20*). Additionally, the 2′-P-AMP binding site contributes to the determination of NADP$^+$/H specificity and coenzyme orientation for HT [particularly, Ser223 and Tyr235 in *Anabaena* FNR (*An*FNR)] (Figure 1) (*2, 21, 22*). Substitutions in equivalent residues of the 2′-P-AMP binding site were efficient in specificity reversion in other flavoenzymes (*9, 10, 23*), but mutations in FNR have been unable to improve NAD$^+$/H-dependent activities. The loops of residues 155−160 and 261−268 (Figure 1), which accommodate the coenzyme pyrophosphate portion, also confer specificity for NADP$^+$/H in *An*FNR (*11, 19*). Selected mutations at Thr155, Ala160, and Leu263, either individually or in combination, produced for the first time FNRs appar-

[†] This work was supported by Ministerio de Educación y Ciencia, Spain (Grant BIO2007-65890-C02-01 to M.M.) and by CONSI+D, DGA (Grant PM062/2007 to M.M.).

[‡] Coordinates and structure factors have been deposited in the Protein Data Bank (PDB) as entries 2vyq (T155G/A160T/L263P/Y303S FNR), 2bmw (T155G/A160T/L263P/R264P/G265P FNR), and 2vzl (T155G/A160T/L263P/Y303S FNR in complex with NAD$^+$).

* To whom correspondence should be addressed: Departamento de Bioquímica y Biología Molecular y Celular, Facultad de Ciencias, Pedro Cerbuna 12, Universidad de Zaragoza, 50009 Zaragoza, Spain. Fax: +34 976 762123. Phone: +34 976 762476. E-mail: mmedina@unizar.es.

[§] Universidad de Zaragoza.

[||] J.R.P. and B.H. contributed equally to the manuscript and should both be considered as first authors.

[⊥] Consejo Superior de Investigaciones Científicas.

[1] Abbreviations: FNR, ferredoxin-NADP$^+$ reductase; FNR$_{ox}$, FNR in the fully oxidized state; FNR$_{rd}$, FNR in the hydroquinone-reduced state; DCPIP, 2,6-dichlorophenolindophenol; Fd, Fd$_{rd}$, ferredoxin and in its reduced state; Fld, Fld$_{rd}$, flavodoxin in its hydroquinone-reduced state; WT, wild-type; rmsd, root-mean-square deviation; NMN, nicotinamide mononucleotide portion of NAD(P)$^+$/H; 2′-P-AMP, 2′-phospho-AMP portion of NADP$^+$/H; ET, electron transfer; HT, hydride transfer; CTC, charge transfer complex; k_{ap}, apparent rate constant; PP3, T155G/A160T/L263P FNR; PP3CT, T155G/A160T/L263P/Y303S FNR; PP5, T155G/A160T/L263P/R264P/G265P FNR; PP5CT, T155G/A160T/L263P/R264P/G265P/Y303S FNR; AMP1PP5, T155G/A160T/S223D/L263P/R264P/G265P FNR; AMP2PP5, T155G/A160T/S223D/Y235F/L263P/R264P/G265P FNR; $k_{A>B}$, $k_{B>C}$, and $k_{C>D}$, apparent conversion rate constants derived by global analysis.

10.1021/bi802077c CCC: $40.75
Published on Web 02/16/2009

A

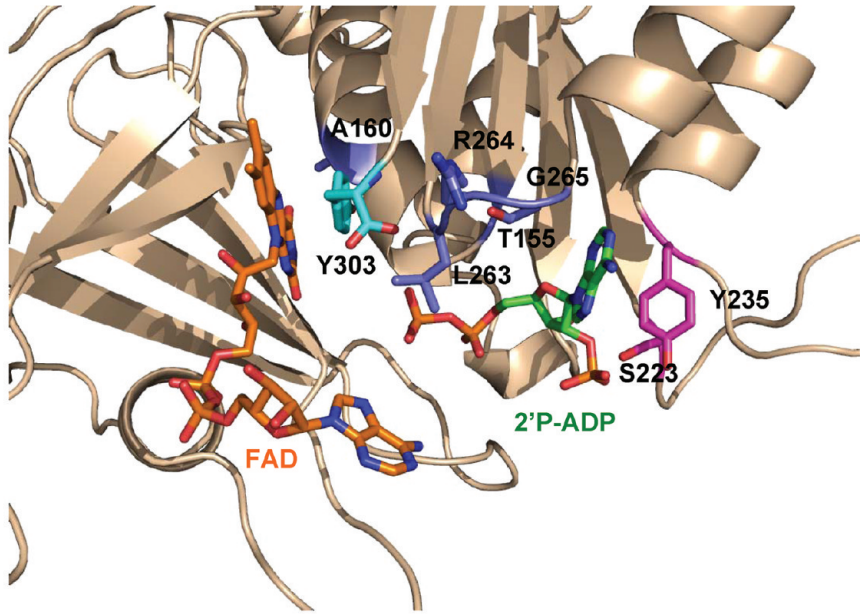

B

				pdb codes
NADPH-DEPENDENT ENZYMES				
*An*FNR	257	HTYICG**L-RG**MEEGIDAALS	274	1que, 1gjr, 2bsa
spFNR	268	YVYMCG**L-KG**MEKGIDDIMV	285	1fnd
pFNR	262	FVYMCG**L-KG**MEKGIDDIMV	279	1qgo, 1qfz, 1qfy
rCYP450R	626	HIYVCG**DARN**MAKDVQNTFY	644	1amo, 1j9z, 1ja0
*Ec*SiR	548	HIYVCG**DANR**MAKDVEQALL	566	1ddi, 1ddg
rNOS	1345	HIYVCG**D-VT**MAADVLKAIQ	1363	1tll
hMTS	646	HIYVCG**DAKN**MAKDVHDALV	665	2qtl, 2qtz
*Pf*FNR	280	ELYICG**H-KS**IRYKVMDIVK	298	2ok8, 2ok7
NADPH,NADH-DEPENDENT ENZYMES				
rcNR	199	IALVCG**PP-A**MIECTVRPGL	217	
NADH-DEPENDENT ENZYMES				
lcNR	589	LALACG**PP-P**MIQFAISPNL	607	2cnd
rCb5R	269	LVLMCG**PP-P**MIQYACLPNL	287	1i7p, 1ib0
piCb5R	241	LVLMCG**PP-P**MIQYACLPNL	259	1ndh
hCb5R	269	LVLMCG**PP-P**MIQYACLPNL	287	1umk
UQR	379	EYYMCG**PG-P**MAN-AVKGML	396	2r6h
*Pc*PDR	195	HVYCCG**PQAL**MDT-VRDMTG	213	2pia

FIGURE 1: (A) Cartoon structure around the *An*FNR active center showing in CPK sticks the regions involved in coenzyme specificity and analyzed in this study. Residues interacting with the 2′-P-AMP and pyrophosphate binding regions are colored magenta and blue, respectively. The C-terminal Tyr is colored cyan. FAD and 2′-P-ADP are drawn in CPK sticks with carbons colored green and orange, respectively. (B) Structural sequence alignment of different members of the FNR superfamily in the region involved in binding of the coenzyme pyrophosphate portion. For those members for which a three-dimensional structure has not been reported, the alignment corresponds to the primary sequence one. The alignment includes FNRs from *Anabaena* PCC 7119 (*An*FNR) (*1*), spinach (spFNR) (*1*), pea (pFNR) (*17*), and *Plasmodium falciparum* (*Pf*FNR) (*12*); rat cytochrome-P450 reductase (rCYP450R) (*43*); sulfite reductase from *Escherichia coli* (*Ec*SiR) (*44*); rat neuronal nitric oxide synthase (rnNOS) (*45*); human methionine synthase reductase (hMTS) (*41*); root (*46*) and leaf (*27*) corn nitrate reductases (rcNR and lcNR, respectively); rat (*41*), pig (*28*), and human erythrocyte cytochrome b_5 reductases (*47*) (rCb5R, piCb5R, and hCb5R); the F subunit of NADH:ubiquinone oxidoreductase Na translocating (UQR) (*48*); and phthalate dioxygenase reductase from *Pseudomonas cepacia* (*Pc*PDR) (*29*). Residue numbers are shown at the left and right of each sequence. Hyphens denote gaps introduced to improve alignment.

ently able to bind NAD^+ (*2, 14, 19*). Finally, a conserved aromatic side chain stacks the *re* face of the flavin, playing a critical role in modulating $NADP^+$/H biding affinity and selectivity (*3, 5, 7, 12, 14, 24, 25*). In *An*FNR, it is the C-terminal Tyr303. Its contribution to lowering the affinity of FNR for $NADP^+$/H, to stabilizing the flavin semiquinone, and to modulating the enzyme midpoint potential and, therefore, the rates of electron and hydride exchange has been proven (*5, 26*).

We have further modeled the $NADP^+$ pyrophosphate binding surface in *An*FNR to mimic that in NAD^+/H-dependent enzymes and to improve our understanding of the parameters determining coenzyme specificity and substrate localization in the active site. NAD^+/H-dependent members of the family present a proline-rich loop in the NAD^+/H pyrophosphate binding site (Figure 1B) (*8, 27*−*29*) that has been introduced here in *An*FNR. FNR forms combining mutations in the pyrophosphate binding region (PP) and in either Tyr303 (CT) or the 2′-P-AMP (AMP) binding site have also been produced. T155G/A160T/L263P/R264P/G265P FNR (PP5) binds $NADP^+$ more weakly than WT FNR, does not form charge transfer complexes (CTCs), and presents a reduced efficiency. T155G/A160T/L263P/Y303S FNR (PP3CT) binds $NADP^+$ and NAD^+ and allows flavin-nicotinamide CTC formation and HT with both coenzymes. Structures of these mutants show how particular coenzyme-binding regions were modeled. However, the "rational redesign" did not improve processes with NAD^+/H, suggesting that coenzyme

specificity in the FNR family might involve determinants difficult to manipulate.

MATERIALS AND METHODS

Oligonucleotide-Directed Mutagenesis and Protein Production. The *An*FNR mutants PP3CT, PP5, T155G/A160T/L263P/R264P/G265P/Y303S (PP5CT), T155G/A160T/S223D/L263P/R264P/G265P (AMP1PP5), and T155G/A160T/S223D/Y235F/L263P/R264P/G265P (AMP2PP5) were produced using the QuikChange mutagenesis kit (Stratagene) (*5*). S223D, Y235F, R264P, G265P, and/or Y303S replacements were introduced into the pET28-T155G/A160T/L263P *An*FNR vector (*19, 30*). Mutations were confirmed by DNA sequence analysis. Mutated pET28-FNRs were expressed in *E. coli* BL21(DE3) Gold cells (Stratagene) and purified as described previously (*19*). UV−visible spectra and SDS−PAGE were used as purity criteria. pET28-PP5CT was unable to express protein, despite the fact that different expression conditions were assayed.

Spectral Analysis. UV−visible spectra were recorded using a Varian Cary-Bio100 instrument. Parameters for interaction between FNR_{ox} mutants and $NADP^+$ or NAD^+ were analyzed by difference absorption spectroscopy at 25 °C in 50 mM Tris-HCl (pH 8.0) (*2, 19*). Errors in K_d and $\Delta\varepsilon$ were ±15%. CD spectra were recorded in a Chirascan spectropolarimeter (Applied Photophysics Ltd.), in 10 mM Tris-HCl (pH 8.0) at 25 °C with 10 μM FNR. Path lengths of 0.1 and 0.4 cm were used for far-UV and near-UV−vis regions, respectively.

Steady-State Enzymatic Assays. FNR steady-state kinetic parameters were determined using the diaphorase assay with 2,6-dichlorophenolindophenol (DCPIP) at 25 °C in 50 mM Tris-HCl (pH 8.0) (*2, 19*). The NADPH activity was assayed using a final FNR concentration of ∼4 nM. An exception was made with mutants containing S223D, which required higher enzyme concentrations (230−540 nM). NADPH concentrations were in the range of 0−0.4 mM for FNRs without the S223D mutation and in the range of 0−4.5 mM when it was included. Higher FNR concentrations were required for reactions with NADH (230−542 nM). The only exception was PP3CT FNR (∼4 nM). The concentration of NADH was in the range of 0−2.6 mM. The kinetic results were interpreted using the Michaelis−Menten model. Estimated errors in K_m and k_{cat} were ±25 and ±10%, respectively.

Pre-Steady-State Kinetic Measurements. Fast HT processes between the FNRs and the $NAD(P)^+$/H coenzymes, as well as electron transfer (ET) between the FNRs and Fd or Fld, were studied by stopped-flow (Applied Photophysics SX.17MV) under anaerobic conditions (*19*) in 50 mM Tris-HCl (pH 8.0). Single-wavelength measurements were carried out at 25 °C using the SX.18MV software and FNR concentrations of ∼10 μM. Measurements simultaneously recorded in the 400−1000 nm range were taken every 2.56 ms at 6 °C using XScan and ∼25 μM FNR (*21*). Reduced proteins were prepared by photoreduction (*26, 31*). The concentrations of $NAD(P)^+$/H coenzymes were in the range of 10−250 μM. Higher coenzyme concentrations were occasionally analyzed for FNRs containing S223D. Single-wavelength apparent rate constants (k_{ap}) were calculated by fitting the data to mono- or biexponential equations. Errors in k_{ap} were ±15%. Time-dependent spectral deconvolution was performed by global analysis and numerical integration methods (Pro-K, Applied Photophysics) (*21*). Data collected from 0.00128−0.05 to 0.00128−2 s were fit to single-step (A > B), two-step (A > B > C), or three-step (A > B > C > D) models, allowing estimation of the apparent conversion rate constants ($k_{A>B}$, $k_{B>C}$, and $k_{C>D}$). The single-step mechanism sometimes applied when part of the reaction occurred within the dead time; therefore, the observed process was notated as B > C. Species A, B, C, and D are spectral species, reflecting a distribution of enzyme intermediates at a certain point along the reaction, and do not necessarily represent a single distinct enzyme intermediate. $k_{A>B}$, $k_{B>C}$, and $k_{C>D}$ denote rates of conversion between these species. The expected species involved are the substrates, products, and the CTCs FNR_{ox}−NADPH (CTC-1) and FNR_{rd}−$NADP^+$ (CTC-2), as previously reported (*21*). In the reaction of PP3CT FNR_{ox} with NADH, the $k_{A>B}$ constant exhibited a saturation dependence, allowing the determination of K_d^{NADH} (*21*). Reactions between FNR_{ox} and Fld_{rd} or Fd_{rd} were followed at 600 and 507 nm, respectively (*26*). Proteins were mixed at a ∼1:1 molar ratio and a final concentration of ∼10 μM.

Crystal Growth, Data Collection, and Structure Refinement. Crystals of PP3CT, PP5, and a complex of PP3CT with NAD^+ were grown by the hanging drop method (Supporting Information). The X-ray data set of PP5 was collected at beamline BM16 of the ESRF (Grenoble, France) on a Marccd detector with a wavelength of 0.97954 Å and a maximum resolution of 1.5 Å. Data sets of PP3CT, free and in complex, were collected using graphite-monochromated Cu Kα radiation generated by Bruker rotating anodes (MICROSTAR or Bruker-Nonius) with PLATINUM 135 CCD and Kappa2000 CCD detectors, respectively.

All crystals belonged to the $P6_5$ hexagonal space group. Unit cell dimensions and other experimental data are detailed in Table SP1 of the Supporting Information. One FNR molecule was found in the asymmetric unit, the V_m values being 2.85, 3.3, and 2.92 $Å^3$/Da for PP3CT, PP5, and the PP3CT−NAD^+ complex, respectively (solvent contents of 56.9, 62.7, and 57.83%, respectively). Data set collection and processing were as indicated in the Supporting Information. The native FNR structure (PDB entry 1que) was used as the search model. Refinement of structures was performed with CNS (*32*), REFMAC 5.0 (*33*), and manual model building with O (*34*). The PP3CT and PP5 models comprised residues 9−303, one FAD, one SO_4^{2-} molecule, and 508 and 586 solvent molecules, respectively. The PP3CT−NAD^+ complex consisted of residues 9−303, one FAD, one NAD^+, and 430 solvent molecules. PROCHECK (*35*) and WHATCHECK (*36*) were used to assess the quality of the final structures. The presence of NAD^+ in the PP3CT−NAD^+ complex was confirmed by $F_o - F_c$ simulated annealing omit map calculation by CNS (*32*).

RESULTS

*Expression and Purification of the FNR Mutants. An*FNR mutants exhibited protein yields, as well as UV−vis and CD spectral properties, similar to those of WT. Therefore, the mutations did not prevent either the assembly of the FAD or protein folding. Nevertheless, PP3CT exhibited UV−vis spectral maxima slightly shifted to shorter wavelengths relative to WT (273, 387, and 455 nm) and weaker intensities

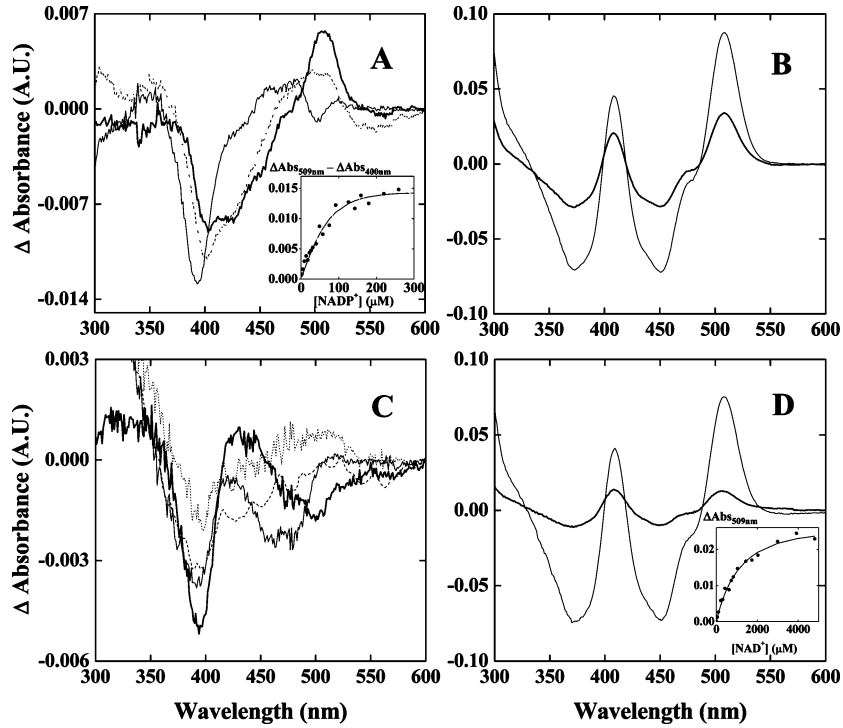

FIGURE 2: Difference absorbance spectra elicited by titration of (A) WT (solid thin line) (31 μM) with $NADP^+$ (89 μM), PP3 (dashed line) (60 μM) with $NADP^+$ (700 μM), and PP5 (solid thick line) (61 μM) with $NADP^+$ (415 μM). The inset shows the saturation profile for the titration of PP5 with $NADP^+$. (B) Y303S (solid thin line) (25 μM) with $NADP^+$ (25 μM) and PP3CT (solid thick line) (26 μM) with $NADP^+$ (28 μM). (C) PP3 (solid thin line) (61 μM) with NAD^+ (2.5 mM), PP5 (solid thick line) (66 μM) with NAD^+ (3.3 mM), AMP1PP5 (dashed line) (62 μM) with NAD^+ (1.4 mM), and AMP2PP5 (dotted line) (58 μM) with NAD^+ (1.8 mM). (D) Y303S FNR (solid thin line) (25 μM) with NAD^+ (5 mM) and PP3CT (solid thick line) (25 μM) with NAD^+ (2.5 mM). The inset shows the saturation profile for the titration of PP3CT with NAD^+.

for positive and negative signals at 273 and 286 nm in the near-UV CD (*2, 30*). This is in agreement with the loss of the interaction of the flavin ring with Tyr303 (*37*). This mutant had a high affinity for $NADP^+$ during purification, as Y303S (*5, 14*), showing displacement of its maxima (271, 401, and 472 nm when $NADP^+$ is bound). Removal of the coenzyme was achieved with an affinity Cibacron-blue column (*30*). Attempts to express PP5CT were unsuccessful. The lack of stability in the 260s loop was also reported in pea FNR mutants (*20*).

Interaction of FNR_{ox} Mutants with $NADP^+$ and NAD^+. Despite the fact titration of PP5 FNR_{ox} with $NADP^+$ produced a difference spectrum with a maximum at 509 (Figure 2A), the pattern of the spectrum was different from that expected for a stacking interaction between the NMN portion of $NADP^+$ and the isoalloxazine. However, the appearance of the band at 509 nm suggests a modification of the flavin environment with regard to WT. Saturation of the difference spectra with an increase in $NADP^+$ concentration allowed determination of $K_d^{NADP^+}$ and $\Delta\varepsilon$ (Figure 2A, inset, and Table 1). $K_d^{NADP^+}$ values were 3.7- and 2-fold weaker than for WT and T155G/A160T/L263P (PP3), respectively (*19*), and $\Delta\varepsilon_{509}$ indicated low occupancy (if any) of the isoalloxazine environment by the nicotinamide (*5*). Titration of PP3CT with $NADP^+$ (Figure 2B) produced spectral perturbations consistent with NMN−flavin stacking (*5*). However, binding was 1 order of magnitude weaker, with a lower level of stacking, than for Y303S FNR (Table 1). Addition of mutations at the 2′-P site to PP5 prevented difference spectra upon $NADP^+$ titration, indicating that $NADP^+$ hardly binds to these mutants.

Table 1: Dissociation Constants for Formation of a Complex of WT and Mutated *An*FNR Forms

FNR	$K_d^{NADP^+}$ (μM)	$\Delta\varepsilon_{509}{}^{NADP^+}$ (mM^{-1} cm^{-1})	$K_d^{NAD^+}$ (μM)	$\Delta\varepsilon_{509}{}^{NAD^+}$ (mM^{-1} cm^{-1})
WT[a]	5.7		nd[b]	
Y303S[c]	≪0.01	3.5	550	3.0
L263P[e]	40		nd	
PP3[d]	43.0		nd	
PP3CT	≪0.1	2.9	1341	1.4
PP5	21.3	0.2	nd[e]	
AMP1PP5	nd[b]		nd[e]	
AMP2PP5	nd[b]		nd[e]	

[a] Data from refs *2* and *31*. [b] No difference spectra have been observed. [c] Data from ref *5*. [d] Data from ref *19*. [e] Very weak difference spectrum signals, which do not allow estimation of K_d.

The WT FNR spectrum remains unaltered upon addition of NAD^+ (*2*). PP5 elicited a weak difference spectrum similar to that reported for PP3 and to that observed for the WT FNR−$NADP^+$ interaction (*19*) (Figure 2A,C). Therefore, although binding is produced, there is no proof for a stacking at the active site. Addition of the S223D and Y235F mutations produced a less defined difference spectrum (Figure 2C). NAD^+ titration of PP3CT (Figure 2D) elicited a spectrum similar to that obtained with $NADP^+$ (Figure 2B), suggesting interaction between the nicotinamide and the isoalloxazine. Small changes in the band positions suggest differences in the interaction (Figure SP1A). $K_d^{NAD^+}$ and $\Delta\varepsilon$ indicate weaker interaction and a lower level of occupancy than those for Y303S (Figure 2D and Table 1).

Steady-State Kinetic Parameters of the FNR Mutants. PP5 and PP3CT exhibited a k_{cat}^{NADPH} in the diaphorase activity half of that of WT. The K_m^{NADPH} increased for PP5, while introduction of the Y303S mutation into PP3 to produce

Table 2: Steady-State Kinetic Parameters for the DCPIP Diaphorase Activity for WT and Mutated *An*FNR Forms

	NADPH			NADH			
FNR	K_m (μM)	k_{cat} (s^{-1})	k_{cat}/K_m^f (s^{-1} μM^{-1})	K_m (μM)	k_{cat} (s^{-1})	k_{cat}/K_m^f (s^{-1} μM^{-1})	specificity for NADPH
WT[a]	6	81.5	13.5	800	0.16	2×10^{-4}	67500
Y303S[b]	1.1	2.8	2.5	48	93	1.9	1.3
L263P[c]	19	17	0.9	650	0.05	8×10^{-5}	11688
PP3[c]	12	77	6.4	390	0.33	8×10^{-4}	7619
PP3CT[d]	4.1	38.5	9.4	39.4	31	0.8	11.75
PP5	23	35	1.5	64	0.65	1.4×10^{-3}	1071
AMP1PP5	1366	3×10^{-4}	2×10^{-7}	1323	8×10^{-3}	6×10^{-6}	
AMP2PP5	*e*	*e*	*e*	1250	5×10^{-4}	4×10^{-7}	

[a] Data from ref *2*. [b] Data from ref *5*. [c] Data from ref *19*. [d] Data from ref *30*. [e] Kinetic parameters could not be estimated due to the very small extension of the reaction. [f] Estimation of enzyme efficiency when the coenzyme concentration was zero (*20*).

Table 3: Single-Wavelength Fast Kinetic Parameters for the Reduction of the Different *An*FNR Forms by NADPH and NADH as Obtained by Stopped-Flow[a]

	NADPH		NADH		Fd_{rd}	Fld_{rd}
FNR	k_{ap1} (s^{-1})	k_{ap2} (s^{-1})	k_{ap1} (s^{-1})	k_{ap2} (s^{-1})	k_{ap2}[h] (s^{-1})	k_{ap2}[h] (s^{-1})
WT[b]	500	200	0.35	0.005	<400	<400
Y303S[c]	460	18.8	420	67	<600	<600
L263P[d]	16	3	0.04			
PP3[d]	<400	130	0.43			
PP3CT[e]	<500	222	24		<400	<400
PP5	80[e]		0.18[f]		<400	157
AMP1PP5[e]	0.21[g]		0.82[f]	0.3[f]	<400	251
AMP2PP5[e]	0.10[g]	0.02[g]	0.4[f]	0.1[f]	400	248

[a] All the reactions were carried out in 50 mM Tris-HCl (pH 8.0) at 25 °C with final protein concentrations of 10 μM and followed at 460 nm for FNRs and NAD(P)H, 507 nm for FNRs and Fd, and 600 nm for FNRs and Fld. [b] Data from ref *2*. [c] Data from ref *5*. [d] Data from ref *19*. [e] Final concentration for NAD(P)H of 10 μM. [f] Reactions studied with the coenzyme at a final concentration of 100 μM. [g] Reactions studied with the coenzyme at a final concentration of 2.3 mM. [h] An important part of the reaction takes place within the dead time, usually allowing only k_{ap2} determination.

PP3CT restored the strength of the enzyme−coenzyme interaction (Table 2). Thus, the catalytic efficiency of PP3CT was in the WT range, but that of PP5 was reduced, in agreement with its lack of stacking. PP5 increased k_{cat}^{NADH} with regard to PP3, while its K_m^{NADH} was similar (Table 2). PP3CT increased k_{cat}^{NADH} and decreased K_m^{NADH} with regard to those of WT. Thus, for both mutants, the catalytic efficiency was improved with regard to that of WT (Table 2) and the specificity for NADPH decreased, particularly in PP3CT (Table 2). FNR mutants including mutations in the 2′-P binding site were highly impaired with both coenzymes (Table 2).

Fast Kinetics Studies of the Reactions of the FNR Mutants with NADP$^+$/H and NAD$^+$/H. Reaction of WT FNR with NADPH produces a fast biexponential absorption decrease at 460 nm, related to the formation of the FNR_{ox}−NADPH complex followed by HT from NADPH to FAD (*21, 38, 39*). The kinetic traces at 460 nm for the reaction with PP5 fit to a considerably slow monoexponential process (Table 3 and Figure SP1B of the Supporting Information). However, the reaction of PP3CT showed a k_{ap} similar to that of WT FNR and improved with regard to those of the PP3 and Y303S mutants (Table 3 and Figure SP1B of the Supporting Information). The reaction of WT FNR, and of most of the mutants reported to the date, with NADH is extremely slow (*2, 5, 19*). The only exception is Y303S FNR (*5*). Kinetic traces for the reaction of PP5 fit a monoexponential process as slow as that of WT (Table 3 and Figure SP1C of the Supporting Information), while the PP3CT mutant exhibited a rate 2 orders of magnitude faster (Table 3). Introduction of the S223D and/or Y235F mutations practically abolished HT from NADPH to FNR, while HT from NADH remained in the low WT levels.

Reactions of PP5 and PP3CT variants with NAD(P)$^+$/H were further analyzed in the 400−1000 nm range (Figure 3). Processes of PP5 were considerably slow, with very small amplitudes and detection of minor traces of CTCs. Reaction of PP3CT FNR_{ox} with NADPH produced a long-wavelength band attributed to a CTC interaction between FNR_{ox} and NADPH (CTC-1) within the dead time (Figure 3A) (*21*). Subsequent evolution of flavin band I, indicating FNR reduction, was concomitant with the appearance of a 800−900 nm band corresponding to FNR_{rd}−NADP$^+$ CTC (CTC-2) in equilibrium with CTC-1 (Figure 3A and Table 4). The first recorded spectrum after NADP$^+$ was mixed with PP3CT FNR_{rd} was consistent with fast association of FNR_{rd} with NADP$^+$ to produce CTC-2 (*21*). It evolved with a negligible increase in the intensity of flavin band I while slightly decreasing the intensity of CTC-2 (Figure 3B).

Reaction of PP3CT FNR_{ox} with NADH fit an A > B > C model. The first species after mixing was consistent with the presence of FNR_{ox} and traces of CTC-1 (568 nm) but rapidly evolved (Table 4 and the inset of Figure 3C). $k_{A>B}$ for this process exhibited a saturation dependence on the NADH concentration, allowing estimation of a K_d^{NADH} of ~30 μM. B indicated further accumulation of CTC-1, reduction of band I, and the appearance of CTC-2 (Figure 3C, inset). B evolved by decreasing the amount of CTC-1 accompanied by a considerable reduction in the amount of FNR with a coenzyme concentration-independent rate constant (Table 4). Reduction of NAD$^+$ by PP3CT FNR_{rd} also fit to an A > B > C model (Figure 3D). A was consistent with free FNR_{rd} in equilibrium with FNR_{ox} traces. Evolution of A was linearly dependent on the coenzyme concentration ($k_2 \sim 1$ μM^{-1} s^{-1}). B showed a slight increase in the absorption at 460 nm and the appearance of CTC-2 (798 nm) and evolved in a coenzyme concentration-independent process with the appearance of traces of FNR_{ox} and a decrease in the level of CTC-2.

Processes of WT FNR_{ox} and FNR_{rd} with NAD$^+$/H were extremely slow (Table 4), without the appearance of any CTC interaction. Y303S FNR_{ox} reacted with NADH through an A > B > C > D model, corresponding to the fast formation of CTC-1, followed by FNR reduction to CTC-2 that evolved toward release of NAD$^+$ once HT takes place (decrease in the magnitude of the CTC-2 band) ($k_{A>B} > 380$ s^{-1}; $k_{B>C} \sim$

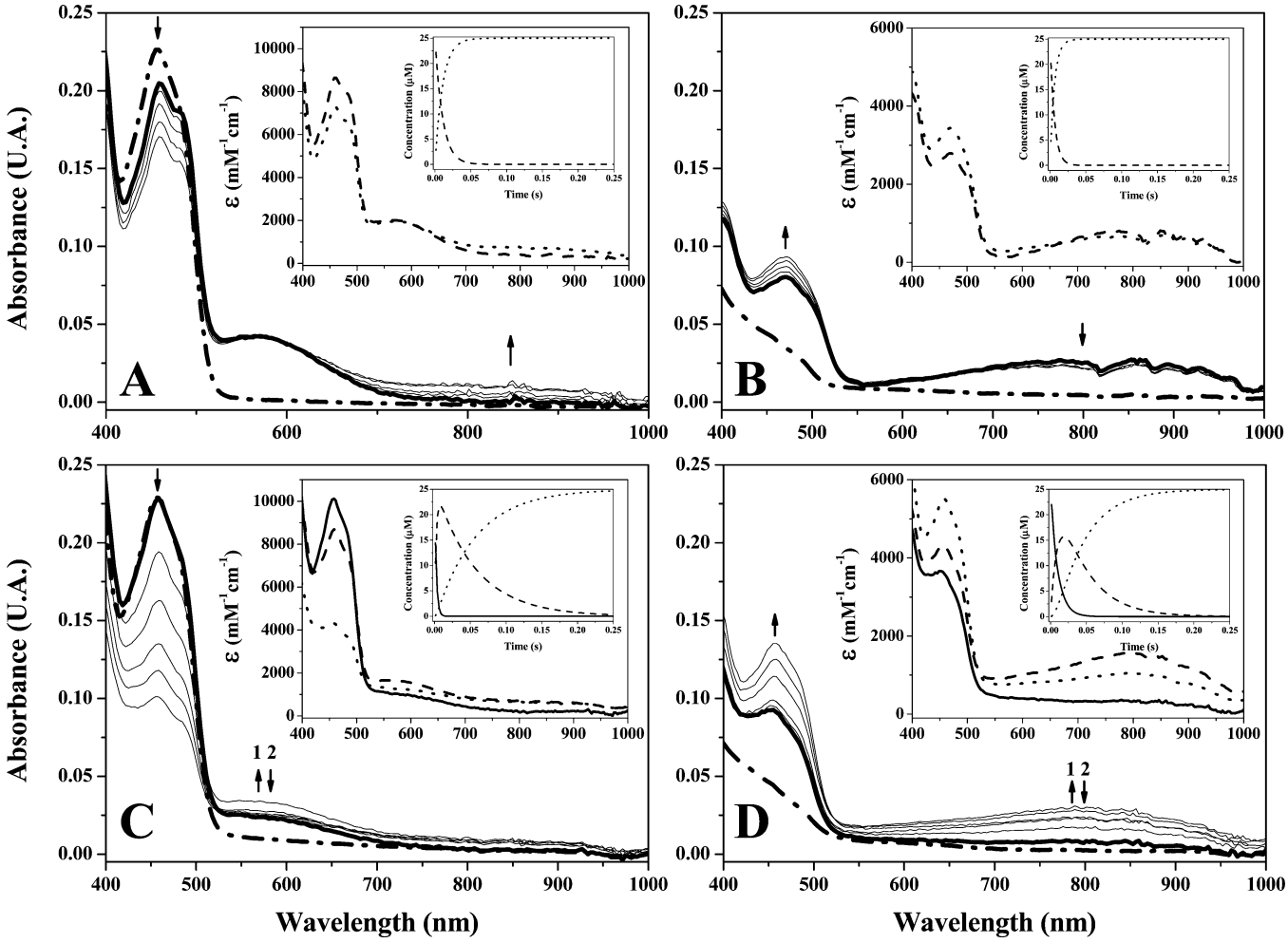

FIGURE 3: Evolution of spectral changes accompanying the reactions of PP3CT with NAD(P)$^+$/H. (A) Time course for the reaction of mutated FNR_{ox} with NADPH. Spectra after mixing are shown at 0.00128, 0.00384, 0.0064, 0.02176, and 0.25 s. (B) Time course for the reaction of mutated FNR_{rd} with $NADP^+$. Spectra after mixing are shown at 0.00128, 0.00384, 0.0064, 0.01152, and 0.25 s. (C) Time course for the reaction of mutated FNR_{ox} with NADH. Spectra after mixing are shown at 0.00128, 0.01152, 0.032, 0.06528, 0.1037, and 0.25 s. (D) Time course for the reaction of mutated FNR_{rd} with NAD^+. Spectra after mixing are shown at 0.00128, 0.00384, 0.00896, 0.02432, 0.05248, and 0.25 s. In all cases, the protein concentration was 25 μM and the coenzyme concentration 125 μM. The corresponding initial oxidized or reduced protein spectrum before mixing is shown as a dashed−dotted line in each figure, and the first spectrum after mixing is shown as a bold line. Directions of absorbance changes are indicated by an arrow with numbers that indicate the sequential direction of the evolution of the absorbance. The corresponding insets show the absorbance spectra for the pre-steady-state kinetically distinguishable species obtained by global analysis of the reactions and the second insets the evolution of these species over time. Data for intermediate A, B, and C species are denoted with bold, dashed, and dotted lines, respectively.

Table 4: Multiple-Wavelength Globally Fit Fast Kinetic Parameters for the Reactions of Different *An*FNR Forms with NAD(P)$^+$/H As Obtained by Stopped-Flow[a]

	NADPH	NADP$^+$	NADH		NAD$^+$	
FNR	$k_{B>C}$[b] (s^{-1})	$k_{B>C}$[b] (s^{-1})	$k_{A>B}$ (s^{-1})	$k_{B>C}$ (s^{-1})	$k_{A>B}$ (s^{-1})	$k_{B>C}$ (s^{-1})
WT	<250[c]	<300[c]	0.02		0.1	
PP3CT	92	181[d]	278	18	102	24
PP5	28			0.13		

[a] All the parameters here reported were obtained in 50 mM Tris/HCl, pH 8.0 at 6°C with final protein concentrations of 25 μM with coenzyme concentrations 125 μM and globally fit by numerical integration methods. [b] The first reaction takes place within the instrument dead time and the process fits better to a B > C single step. [c] Data from (*21*). [d] Almost no amplitude is observed for the process.

250 s^{-1}, and $k_{C>D} \sim 30$ s^{-1}) (Figure SP2A). The reverse reaction occurred through a two-step mechanism (Figure SP2B), with a behavior similar to that observed for the reaction of PP3CT FNR_{rd} with NAD^+ and with $k_{A>B}$ also linearly dependent on the coenzyme concentration ($k_2 \sim 0.7$ μM^{-1} s^{-1}).

Fast Kinetics Reduction of FNR Mutants by Its Protein Partners, Fd and Fld. Reduction of all FNR mutants by Fd_{rd} was very fast, indicating they were able to efficiently interact with and accept electrons from Fd_{rd}. Slightly slower processes were observed for the reduction by Fld_{rd} (Table 3) (*26*), consistent with the larger contribution of the $NADP^+$ domain to the interaction with Fld (*13*).

Three-Dimensional Structures of the FNR Variants. The structures of PP3CT and PP5 did not present significant differences with regard to WT FNR (C_α backbone rmsd of 0.27 and 0.32 Å, respectively) (Figure 4A). None of the mutants containing the S223D mutation produced crystals. The mutations provoked a retraction in the 261−265 loop conformation, particularly in PP5 (Figure 4A) where the loop deviated with regard to WT, PP3CT, and the WT FNR−$NADP^+$ complex by 1.06, 0.82, and 0.73 Å, respectively. Thus, this structure resembled that of the WT FNR−$NADP^+$ complex in the 260s loop (Figure SP3 of the Supporting Information) (*11*). This led to the loss of the

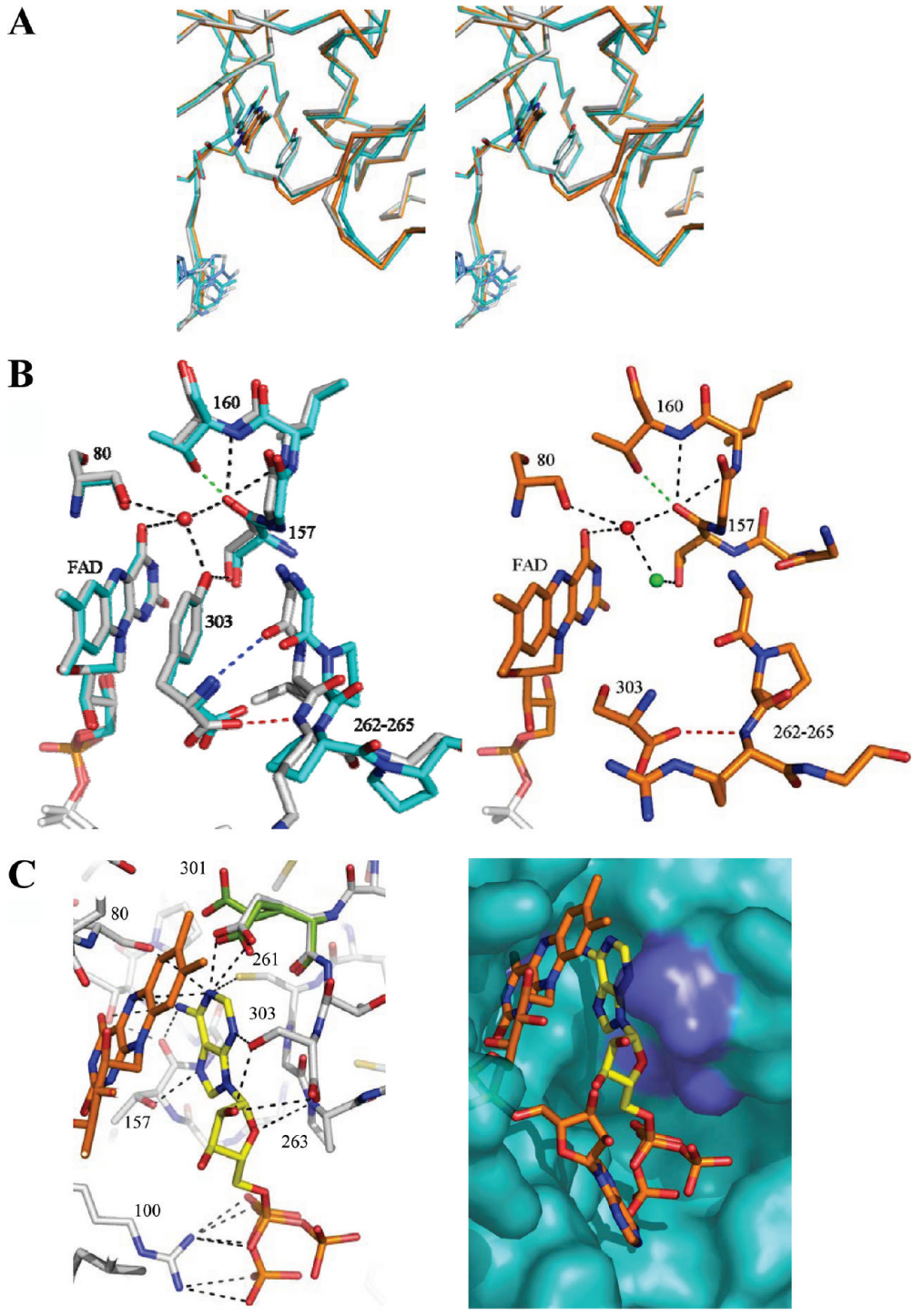

FIGURE 4: Comparison of the three-dimensional structures of the different FNR forms in the FAD environment and the pyrophosphate binding region. (A) Ribbon superposition. (B) Detail of the H-bond networks: red, in only WT and PP3CT; blue, in only WT and PP5; green, in only PP3CT and PP5; black, in all structures. WT is colored gray, PP5 blue, and PP3CT orange. (C) Interaction of NAD$^+$ with PP3CT. The two alternative conformations for the Glu301 chain in PP3CT are colored green in the left panel. The right panel shows a detail of the fittings of the AMP portion of NAD$^+$ into the PP3CT active site (positions bearing mutations are indicated by a violet surface). FAD, NADP$^+$, and the AMP portion of NAD$^+$ are shown in CPK sticks with carbons colored orange, pink, and yellow, respectively. P atoms are colored orange for both coenzymes.

H-bond between one of the terminal carboxylate O atoms and the main chain N atom of Arg264 in PP5, while the H-bond between the N atom of Tyr303 and the O group of Gly262 disappeared in PP3CT (Figure 4B). Mutations at positions 155 and 160 produced additional effects (*19*). A Thr at position 160 allowed the formation of a H-bond between its OH group and the main chain O of Thr157, as reported for PP3 (*19*). Finally, upon replacement of Tyr303 with Ser in PP3CT, a water network partially replaces the position of Tyr303 and a water molecule keeps the H-bonds formed by the Tyr OH group in the WT (Figure 4B).

Arg100 shows in the PP3CT and PP5 structures the same conformation found in Y303S FNR. It is intermediate between those of WT free and in complex with NADP$^+$ (Figure SP4A of the Supporting Information), standing part of its guanidinium group in the space where the pyrophos-

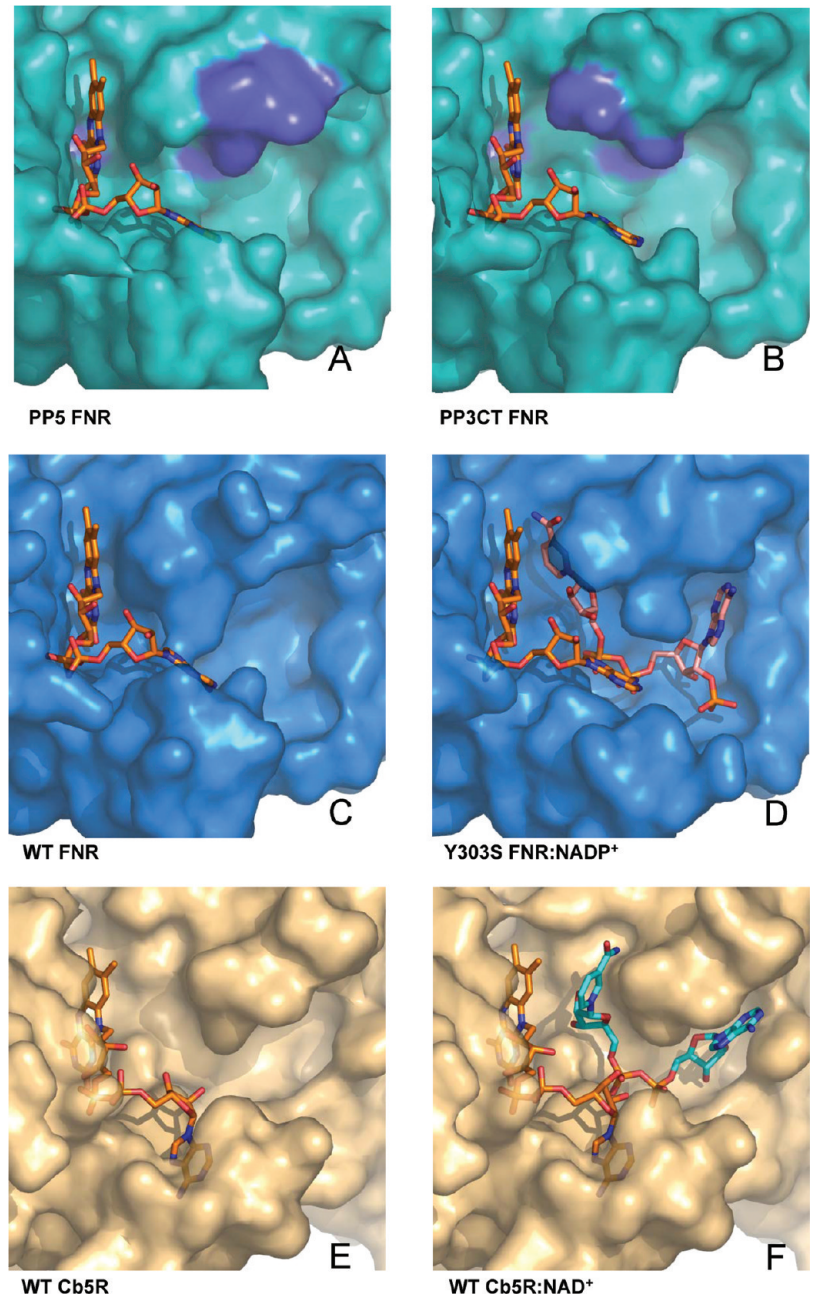

FIGURE 5: Conformation of the enzyme surface at the coenzyme binding pocket for (A) PP5, (B) PP3CT, (C) WT FNR (PDB entry 1que) (*16*), (D) the Y303S FNR−$NADP^+$ complex (PDB entry 2bsa) (*5*), and cytochrome b_5 reductase (E) free (PDB entry 1l7p) and (F) in complex with NAD^+ (PDB entry 1ibo) (*41*). FAD, $NADP^+$, and NAD^+ are shown in CPK sticks with carbons colored orange, pink, and blue, respectively. In structures A and B, positions bearing mutations are indicated by a violet surface.

phate moiety of $NADP^+$ should bind (*5, 16, 40*). A change in the conformation of this chain has been shown to be essential for H-bonding to the $NADP^+$ pyrophosphate bridge (*11, 40*). The high resolution allowed discrimination between two alternative conformations for Gln237, Met266, and Glu301 in PP3CT (Figure 4C) and also suggested such a possibility for Thr302 and Ser303.

Cocrystallization of PP3CT with either NAD^+ or $NADP^+$ yielded crystals with only NAD^+. The overall FNR folding was similar to that of the free mutant (rmsd of the C_α backbone of 0.50 Å). The electron density map assigned to NAD^+ showed strong densities for the adenine and the pyrophosphate. The calculated $F_o - F_c$ omit map at 2.5σ confirmed the presence and conformation of the NAD^+ inside the binding site in a fashion very different from that expected in WT (Figure SP4B of the Supporting Information). Since no crystal packing interactions were observed in this region, this structure appears to be a binding mode stabilized in the crystallization conditions that might be somehow populated in solution at the pH at which the crystals were grown. The adenine of the coenzyme stacked against the *re* face of the FAD pyrazine, in the cavity in which the nicotinamide would be expected (Figures 4C and SP5 of the Supporting Information) (*5, 11*). The second conformation of Glu301 stabilized the position of the adenine by forming two H-bonds with N1. Other nitrogens of the adenine make H-bonds with Thr157, Gly158, Cys261, and Ser303 (Figure 4C). Two conformations are observed for the pyrophosphate moiety of NAD^+, stabilized by Arg100 (Figure 4C). The electron density map corresponding to the nicotinamide portion was

not visible. This can be attributed to multiple conformations in the crystal molecules.

DISCUSSION

We have modeled the *An*FNR $NADP^+$ pyrophosphate binding surface by producing the PP5 and the PP3CT variants. Despite both mutants being able to interact with $NADP^+$ and NAD^+, PP5 does not appear to allow flavin−nicotinamide interactions efficient for HT (Figure 2A and Table 1). The structure of PP5 shows changes in the H-bond network with regard to WT, which, together with less conformational freedom of the prolines and the removal of Leu263 and Arg264 chains, produces a compact conformation of the 260s loop (Figures 4B and 5A). Thus, a displacement of the 260s loop with regard to WT FNR, L263P FNR, and PP3 (Figure SP3 of the Supporting Information) (*2, 19*), as well as a broader binding cavity, is observed (Figure 5A,C). However, this mutant binds $NADP^+$ more weakly than WT, and there is no evidence of better nicotinamide stacking (Figure 2A and Table 1). Displacement of the 260s loop also produced the weakening of the H-bond interactions between Tyr303 and the 261−265 loop (Figure 4), a feature conserved in most of the FNR-like $NADP^+$/H-dependent members (*5, 11*). Therefore, nesting of the nicotinamide in the active site in WT might be somehow favored by the H-bonds connecting the terminal carboxylate and the 260s loop, although the underlying mechanism is still unknown. Altogether, these structural modifications might be related to the reduced catalytic efficiency and HT rates (Tables 2 and 3). This suggests that substrate orientation in the WT active site might be induced by recognition through its 2′-AMP (*2, 21*), but also through the geometry of the 260s loop and the changes induced to adapt the coenzyme pyrophosphate (*11, 20*).

The surface conformation around the 260s loop of PP5 resembles that of NAD^+/H-dependent members (Figure 5A,E,F) (*41*). Despite the fact that these features might explain the weak binding to NAD^+ (Table 2 and Figure 2C), they do not correlate with an enhancement of reactivity (Tables 3 and 4). Therefore, the transfer of sequence motifs did not work as expected. This might be due to the new cavity being unable to complement the shape and charge of the coenzyme. Additionally, since NAD^+-dependent members have a slightly different NAD^+ domain to FAD domain relationship, which we did not redesign, nonadequate domain−domain relationships might be also behind the lack of activity.

The PP3CT structure shows a coenzyme binding cavity even broader than that of PP5 (Figure 5B), with the 260s loop and C-terminal Tyr connected through only one of the two H-bonds present in WT (Figure 4B). Its complex with NAD^+ showed an unexpected relationship between the flavin and the coenzyme (Figure 4C). Since close flavin−nitotinamide stacking and CTCs are observed for processes with PP3CT, this nonproductive complex must represent a minor contribution in solution (Figures 2 and 3). However, it suggests that the wider cavity might allow different dispositions of the nicotinamide in the active site, in agreement with the decrease in the HT efficiency with regard to Y303S (Table 3). Therefore, mutations in the pyrophosphate binding region might allow additional freedom in the active site chains, further contributing to breaking the specificity for the nicotinamide. Thus, PP3CT slightly restores the turnover and catalytic efficiency with NADPH (limited in Y303S by the strong binding and the rate of product dissociation and in PP3 by the weak binding) (*5, 19*) and shows less specificity for NADPH than WT (Table 2). Finally, HT from reduced PP3CT to $NADP^+$ hardly occurred, in agreement with the less negative reduction potential expected for this variant (*5, 26*).

PP5 was further modified by replacement of S223 and Y235, situated in the AMP binding site, with residues found in NAD^+/H-dependent enzymes (Figure 1) (*2*). The produced mutants were not catalytically efficient with either $NADP^+$/H or NAD^+/H (Tables 1−4). This is in agreement with residues at the 2′-P-AMP site providing coenzyme binding energy (*4, 13*), as well as allocating the 2′-P-AMP moiety to induce the conformational changes required to reach an optimal disposition of the nicotinamide for HT (*2, 11, 21*).

Therefore, so far, only FNR mutants including the Tyr303 to Ser mutation are reported to produce CTCs with NAD^+/H and to show some HT ability with this coenzyme. The mutations introduced into the FNR pyrophosphate binding site modeled particular regions of the coenzyme binding cavity, making them more similar to those of NAD^+/H-dependent members of the family (Figure 5). However, they are far from being perfectly adapted to NAD^+. In fact, the final effect produced when mutations are combined in FNR is difficult to predict. It might be also that the NAD^+-specific motifs work well only in the context of a particular FAD domain to NAD^+ domain relationship. In conclusion, protein regions far from the active center, but involved in the protein interaction with the 2′-P-AMP and pyrophosphate, suffer conformational changes upon coenzyme interaction. These structural changes are sensed by the active center, being the HT efficiency dependent on the correct orientation between the reacting atoms. Therefore, it is feasible to think that the proteins of the FNR family have adapted their $NAD(P)^+$ binding site to interact with the pyridine nucleotide coenzymes modulating the flavin−nicotinamide interaction to unique orientations. In this way, FNR-like domains can adapt to the coenzyme oxidation or reduction rates required in each particular ET chain where they work. We still need to identify these additional parameters involved in structure−function relationships to understand the implication of different protein regions in the catalytic mechanism. Thus, the "rational approach" in the redesign of the coenzyme specificity in the FNR family is more complex than initially expected.

ACKNOWLEDGMENT

We thank Dr. I. Pérez-Dorado for her helpful and invaluable assistance and discussion during resolution of three-dimensional structures. We also thank C. Hamiaux and B. Schierbeek from Bruker for collecting and partially processing the X-ray data for PP3CT FNR.

SUPPORTING INFORMATION AVAILABLE

Protein crystal growth conditions, structure refinement methods, refinement statistics, and figures containing additional biochemical and structural characterization. This material is available free of charge via the Internet at http://pubs.acs.org.

REFERENCES

1. Karplus, P. A., and Bruns, C. M. (1994) Structure-function relations for ferredoxin reductase. *J. Bioenerg. Biomembr. 26*, 89–99.
2. Medina, M., Luquita, A., Tejero, J., Hermoso, J., Mayoral, T., Sanz-Aparicio, J., Grever, K., and Gomez-Moreno, C. (2001) Probing the determinants of coenzyme specificity in ferredoxin-NADP$^+$ reductase by site-directed mutagenesis. *J. Biol. Chem. 276*, 11902–11912.
3. Elmore, C. L., and Porter, T. D. (2002) Modification of the nucleotide cofactor-binding site of cytochrome P-450 reductase to enhance turnover with NADH in vivo. *J. Biol. Chem. 277*, 48960–48964.
4. Carrillo, N., and Ceccarelli, E. A. (2003) Open questions in ferredoxin-NADP$^+$ reductase catalytic mechanism. *Eur. J. Biochem. 270*, 1900–1915.
5. Tejero, J., Perez-Dorado, I., Maya, C., Martinez-Julvez, M., Sanz-Aparicio, J., Gomez-Moreno, C., Hermoso, J. A., and Medina, M. (2005) C-Terminal tyrosine of ferredoxin-NADP$^+$ reductase in hydride transfer processes with NAD(P)$^+$/H. *Biochemistry 44*, 13477–13490.
6. Scrutton, N. S., Berry, A., and Perham, R. N. (1990) Redesign of the coenzyme specificity of a dehydrogenase by protein engineering. *Nature 343*, 38–43.
7. Dohr, O., Paine, M. J., Friedberg, T., Roberts, G. C., and Wolf, C. R. (2001) Engineering of a functional human NADH-dependent cytochrome P450 system. *Proc. Natl. Acad. Sci. U.S.A. 98*, 81–86.
8. Marohnic, C. C., Bewley, M. C., and Barber, M. J. (2003) Engineering and characterization of a NADPH-utilizing cytochrome b5 reductase. *Biochemistry 42*, 11170–11182.
9. Rosell, A., Valencia, E., Ochoa, W. F., Fita, I., Pares, X., and Farres, J. (2003) Complete reversal of coenzyme specificity by concerted mutation of three consecutive residues in alcohol dehydrogenase. *J. Biol. Chem. 278*, 40573–40580.
10. Andreadeli, A., Platis, D., Tishkov, V., Popov, V., and Labrou, N. E. (2008) Structure-guided alteration of coenzyme specificity of formate dehydrogenase by saturation mutagenesis to enable efficient utilization of NADP$^+$. *FEBS J. 275*, 3859–3869.
11. Hermoso, J. A., Mayoral, T., Faro, M., Gomez-Moreno, C., Sanz-Aparicio, J., and Medina, M. (2002) Mechanism of coenzyme recognition and binding revealed by crystal structure analysis of ferredoxin-NADP$^+$ reductase complexed with NADP$^+$. *J. Mol. Biol. 319*, 1133–1142.
12. Aliverti, A., Pandini, V., Pennati, A., de Rosa, M., and Zanetti, G. (2008) Structural and functional diversity of ferredoxin-NADP$^+$ reductases. *Arch. Biochem. Biophys. 474*, 283–291.
13. Medina, M., and Gomez-Moreno, C. (2004) Interaction of ferredoxin-NADP(+) reductase with its substrates: optimal interaction for efficient electron transfer. *Photosynth. Res. 79*, 113–131.
14. Piubelli, L., Aliverti, A., Arakaki, A. K., Carrillo, N., Ceccarelli, E. A., Karplus, P. A., and Zanetti, G. (2000) Competition between C-terminal tyrosine and nicotinamide modulates pyridine nucleotide affinity and specificity in plant ferredoxin-NADP$^+$ reductase. *J. Biol. Chem. 275*, 10472–10476.
15. Bruns, C. M., and Karplus, P. A. (1995) Refined crystal structure of spinach ferredoxin reductase at 1.7 Å resolution: Oxidized, reduced and 2′-phospho-5′-AMP bound states. *J. Mol. Biol. 247*, 125–145.
16. Serre, L., Vellieux, F. M., Medina, M., Gomez-Moreno, C., Fontecilla-Camps, J. C., and Frey, M. (1996) X-ray structure of the ferredoxin:NADP$^+$ reductase from the cyanobacterium *Anabaena* PCC 7119 at 1.8 Å resolution, and crystallographic studies of NADP$^+$ binding at 2.25 Å resolution. *J. Mol. Biol. 263*, 20–39.
17. Deng, Z., Aliverti, A., Zanetti, G., Arakaki, A. K., Ottado, J., Orellano, E. G., Calcaterra, N. B., Ceccarelli, E. A., Carrillo, N., and Karplus, P. A. (1999) A productive NADP$^+$ binding mode of ferredoxin-NADP$^+$ reductase revealed by protein engineering and crystallographic studies. *Nat. Struct. Biol. 6*, 847–853.
18. Hurley, J. K., Morales, R., Martinez-Julvez, M., Brodie, T. B., Medina, M., Gomez-Moreno, C., and Tollin, G. (2002) Structure-function relationships in *Anabaena* ferredoxin/ferredoxin:NADP$^+$ reductase electron transfer: Insights from site-directed mutagenesis, transient absorption spectroscopy and X-ray crystallography. *Biochim. Biophys. Acta 1554*, 5–21.
19. Tejero, J., Martinez-Julvez, M., Mayoral, T., Luquita, A., Sanz-Aparicio, J., Hermoso, J. A., Hurley, J. K., Tollin, G., Gomez-Moreno, C., and Medina, M. (2003) Involvement of the pyrophosphate and the 2′-phosphate binding regions of ferredoxin-NADP$^+$ reductase in coenzyme specificity. *J. Biol. Chem. 278*, 49203–49214.
20. Musumeci, M. A., Arakaki, A. K., Rial, D. V., Catalano-Dupuy, D. L., and Ceccarelli, E. A. (2008) Modulation of the enzymatic efficiency of ferredoxin-NADP(H) reductase by the amino acid volume around the catalytic site. *FEBS J. 275*, 1350–1366.
21. Tejero, J., Peregrina, J. R., Martinez-Julvez, M., Gutierrez, A., Gomez-Moreno, C., Scrutton, N. S., and Medina, M. (2007) Catalytic mechanism of hydride transfer between NADP$^+$/H and ferredoxin-NADP$^+$ reductase from *Anabaena* PCC 7119. *Arch. Biochem. Biophys. 459*, 79–90.
22. Aliverti, A., Lubberstedt, T., Zanetti, G., Herrmann, R. G., and Curti, B. (1991) Probing the role of lysine 116 and lysine 244 in the spinach ferredoxin-NADP$^+$ reductase by site-directed mutagenesis. *J. Biol. Chem. 266*, 17760–17763.
23. Tomita, T., Fushinobu, S., Kuzuyama, T., and Nishiyama, M. (2006) Structural basis for the alteration of coenzyme specificity in a malate dehydrogenase mutant. *Biochem. Biophys. Res. Commun. 347*, 502–508.
24. Gutierrez, A., Doehr, O., Paine, M., Wolf, C. R., Scrutton, N. S., and Roberts, G. C. (2000) Trp-676 facilitates nicotinamide coenzyme exchange in the reductive half-reaction of human cytochrome P450 reductase: Properties of the soluble W676H and W676A mutant reductases. *Biochemistry 39*, 15990–15999.
25. Adak, S., Sharma, M., Meade, A. L., and Stuehr, D. J. (2002) A conserved flavin-shielding residue regulates NO synthase electron transfer and nicotinamide coenzyme specificity. *Proc. Natl. Acad. Sci. U.S.A. 99*, 13516–13521.
26. Nogues, I., Tejero, J., Hurley, J. K., Paladini, D., Frago, S., Tollin, G., Mayhew, S. G., Gomez-Moreno, C., Ceccarelli, E. A., Carrillo, N., and Medina, M. (2004) Role of the C-terminal tyrosine of ferredoxin-nicotinamide adenine dinucleotide phosphate reductase in the electron transfer processes with its protein partners ferredoxin and flavodoxin. *Biochemistry 43*, 6127–6137.
27. Lu, G., Lindqvist, Y., Schneider, G., Dwivedi, U., and Campbell, W. (1995) Structural studies on corn nitrate reductase: Refined structure of the cytochrome b reductase fragment at 2.5 Å, its ADP complex and an active-site mutant and modeling of the cytochrome b domain. *J. Mol. Biol. 248*, 931–948.
28. Nishida, H., Inaka, K., Yamanaka, M., Kaida, S., Kobayashi, K., and Miki, K. (1995) Crystal structure of NADH-cytochrome b5 reductase from pig liver at 2.4 Å resolution. *Biochemistry 34*, 2763–2767.
29. Correll, C. C., Batie, C. J., Ballou, D. P., and Ludwig, M. L. (1992) Phthalate dioxygenase reductase: A modular structure for electron transfer from pyridine nucleotides to [2Fe-2S]. *Science 258*, 1604–1610.
30. Martinez-Julvez, M., Tejero, J., Peregrina, J. R., Nogues, I., Frago, S., Gomez-Moreno, C., and Medina, M. (2005) Towards a new interaction enzyme:coenzyme. *Biophys. Chem. 115*, 219–224.
31. Medina, M., Martinez-Julvez, M., Hurley, J. K., Tollin, G., and Gomez-Moreno, C. (1998) Involvement of glutamic acid 301 in the catalytic mechanism of ferredoxin-NADP$^+$ reductase from *Anabaena* PCC 7119. *Biochemistry 37*, 2715–2728.
32. Brunger, A. T., Adams, P. D., Clore, G. M., DeLano, W. L., Gros, P., Grosse-Kunstleve, R. W., Jiang, J. S., Kuszewski, J., Nilges, M., Pannu, N. S., Read, R. J., Rice, L. M., Simonson, T., and Warren, G. L. (1998) Crystallography & NMR system: A new software suite for macromolecular structure determination. *Acta Crystallogr. D54*, 905–921.
33. Murshudov, G. N., Vagin, A. A., and Dodson, E. J. (1997) Refinement of macromolecular structures by the maximum-likelihood method. *Acta Crystallogr. D53*, 240–255.
34. Jones, T. A., Zou, J. Y., Cowan, S. W., and Kjeldgaard, M. (1991) Improved methods for building protein models in electron-density maps and the location of errors in these models. *Acta Crystallogr. A47*, 110–119.
35. Laskowski, R. A., MacArthur, M. W., Moss, D. S., and Thornton, J. M. (1993) PROCHECK: A program to check the stereochemical quality of protein structures. *J. Appl. Crystallogr. 26*, 283–291.
36. Vriend, G. (1990) WHAT IF: A molecular modeling and drug design program. *J. Mol. Graphics 8*, 52–56, 29.
37. Leadbeater, C., McIver, L., Campopiano, D. J., Webster, S. P., Baxter, R. L., Kelly, S. M., Price, N. C., Lysek, D. A., Noble, M. A., Chapman, S. K., and Munro, A. W. (2000) Probing the NADPH-binding site of *Escherichia coli* flavodoxin oxidoreductase. *Biochem. J. 352*, 257–266.

38. Batie, C. J., and Kamin, H. (1984) Electron transfer by ferredoxin: $NADP^+$ reductase. Rapid-reaction evidence for participation of a ternary complex. *J. Biol. Chem. 259*, 11976–11985.
39. Batie, C. J., and Kamin, H. (1984) Ferredoxin:$NADP^+$ oxidoreductase. Equilibria in binary and ternary complexes with $NADP^+$ and ferredoxin. *J. Biol. Chem. 259*, 8832–8839.
40. Martinez-Julvez, M., Hermoso, J., Hurley, J. K., Mayoral, T., Sanz-Aparicio, J., Tollin, G., Gomez-Moreno, C., and Medina, M. (1998) Role of Arg100 and Arg264 from *Anabaena* PCC 7119 ferredoxin-$NADP^+$ reductase for optimal $NADP^+$ binding and electron transfer. *Biochemistry 37*, 17680–17691.
41. Bewley, M. C., Marohnic, C. C., and Barber, M. J. (2001) The structure and biochemistry of NADH-dependent cytochrome b5 reductase are now consistent. *Biochemistry 40*, 13574–13582.
42. Wolthers, K. R., Lou, X., Toogood, H. S., Leys, D., and Scrutton, N. S. (2007) Mechanism of coenzyme binding to human methionine synthase reductase revealed through the crystal structure of the FNR-like module and isothermal titration calorimetry. *Biochemistry 46*, 11833–11844.
43. Wang, M., Roberts, D. L., Paschke, R., Shea, T. M., Masters, B. S., and Kim, J. J. (1997) Three-dimensional structure of NADPH-cytochrome P450 reductase: Prototype for FMN- and FAD-containing enzymes. *Proc. Natl. Acad. Sci. U.S.A. 94*, 8411–8416.
44. Gruez, A., Pignol, D., Zeghouf, M., Coves, J., Fontecave, M., Ferrer, J. L., and Fontecilla-Camps, J. C. (2000) Four crystal structures of the 60 kDa flavoprotein monomer of the sulfite reductase indicate a disordered flavodoxin-like module. *J. Mol. Biol. 299*, 199–212.
45. Garcin, E. D., Bruns, C. M., Lloyd, S. J., Hosfield, D. J., Tiso, M., Gachhui, R., Stuehr, D. J., Tainer, J. A., and Getzoff, E. D. (2004) Structural basis for isozyme-specific regulation of electron transfer in nitric-oxide synthase. *J. Biol. Chem. 279*, 37918–37927.
46. Long, D. M., Oaks, A., and Rothstein, S. J. (1992) Regulation of Maize Root Nitrate Reductase Messenger-RNA Levels. *Physiol. Plant. 85*, 561–566.
47. Bando, S., Takano, T., Yubisui, T., Shirabe, K., Takeshita, M., and Nakagawa, A. (1929) (2004) Structure of human erythrocyte NADH-cytochrome b5 reductase. *Acta Crystallogr. D60*, 1934.
48. Nelson, K. E., Weinel, C., Paulsen, I. T., Dodson, R. J., Hilbert, H., Martins dos Santos, V. A., Fouts, D. E., Gill, S. R., Pop, M., Holmes, M., Brinkac, L., Beanan, M., DeBoy, R. T., Daugherty, S., Kolonay, J., Madupu, R., Nelson, W., White, O., Peterson, J., Khouri, H., Hance, I., Chris Lee, P., Holtzapple, E., Scanlan, D., Tran, K., Moazzez, A., Utterback, T., Rizzo, M., Lee, K., Kosack, D., Moestl, D., Wedler, H., Lauber, J., Stjepandic, D., Hoheisel, J., Straetz, M., Heim, S., Kiewitz, C., Eisen, J. A., Timmis, K. N., Dusterhoft, A., Tummler, B., and Fraser, C. M. (2002) Complete genome sequence and comparative analysis of the metabolically versatile *Pseudomonas putida* KT2440. *Environ. Microbiol. 4*, 799–808.

BI802077C